

The inhomogeneity of vertical distributions of suspended matter in the sea – consequences for remote sensing

OCEANOLOGIA, No. 36 (1)
pp. 47–79, 1994.
PL ISSN 0078–3234

Remote sensing
Suspended matter
Reflectance
AVHRR
Baltic
Gulf of Gdańsk

KATARZYNA BRADTKE,
ADAM KRĘŻEL
Institute of Oceanography,
University of Gdańsk,
Gdynia

Manuscript received March 7, 1994, in final form September 8, 1994.

Abstract

The influence of the vertical variability of suspended matter $C(z)$ within the optical penetration layer on the reflectance $R(\lambda)$ over the sea surface in the southern Baltic and the Gulf of Gdańsk were analysed. Using Gordon and Clark's model the value of reflectance $R(620)$, taken to be representative of AVHRR channel 1, was calculated. Various vertical seston profiles obtained after previous analysis of real distributions of suspended matter in the surface layer of the sea were taken to be input parameters.

The variability of vertical seston distribution on $R(620)$ was found to be negligible except when the surface concentration exceeded 8 mg dm^{-3} and rapidly decreased with depth. In order to estimate the seston content of the sea surface layer using optical remote sensing methods, the best results should be achieved when comparing reflectance with the 'optically-weighted concentration' defined by Gordon and Clarke (1980). Except in areas close to river mouths and other terrestrial sources of seston in the Baltic, the vertical variability of suspended matter within the optical penetration layer (typically a few metres) is rather small. This means that surface measurements of seston concentration can be used to calibrate the $C = f(R)$ relationship.

Using AVHRR channel 1 data it is possible in the southern Baltic to record surface changes in suspended matter concentration of the order of 0.5 mg dm^{-3} .

1. Introduction

The distribution and transport of suspended materials is one of the most important problems in the study of estuaries and many coastal regions. Suspended matter (seston) plays an important role in the primary production

process and is also a transport medium for micropollutants. The monitoring of suspended sediment is fundamental to the solution of many different problems such as the silting up of ports and the sediment balance of enclosed bays.

Several researchers have shown that there is a significant relationship between the concentration of seston in water and radiance data collected by satellite (Munday and Alfoldi, 1979; Ritchie *et al.*, 1987; Tassan and Sturm, 1986). This has increased interest in the use of satellite observations to determine seston content in natural waters. Remote sensing makes possible the synoptic coverage of large areas and frequent repeatability of measurements. This is of great significance in the search for solutions to at least some of the above-mentioned problems.

To provide estimates of total suspended matter in the sea, data collected from radiometers such as the Landsat Multispectral Scanner System (MSS) and Thematic Mapper (TM), the Advanced Very High Resolution Radiometer (AVHRR) aboard NOAA and the Coastal Zone Color Scanner aboard Nimbus 7 are used.

The information obtained from satellite data is subject to limitations due to instrument resolution, orbit direction and altitude, atmospheric conditions (*e.g.* cloudiness) and data processing techniques. The characteristic interaction of electromagnetic waves with sea water also determines for which purposes this data is to be used. The penetration depth of light in the sea varies strongly with wavelength λ . Concentrations estimated from satellite data must be treated as averaged concentrations within the surface layer. Since seston concentration often depends strongly on depth, it is important to understand quantitatively the influence of such vertical stratification on the remotely determined quantity.

Taking into account the optical properties characteristic of the Gulf of Gdańsk water, the aim of the work is to investigate how vertical stratification of the seston profile influences marine reflectance, to evaluate the upper portion of this profile, which strongly influences marine signals received by satellite, and to discuss whether Gordon and Clark's (1980) concept of 'optically weighted concentration' is appropriate in the interpretation of satellite estimations.

2. Theoretical basis of the remote determination of suspended matter in the sea

The upwelling radiation reaching a sensor on board the satellite is the sum of many composite parts arising from the interactions of light with the components of the atmosphere and sea. Part of the irradiance that is of interest to oceanographers is made up of sun and sky light that has been

scattered in the water body. Its wavelength spectrum depends on the characteristics of the interaction of light with the optically active components of water, *i.e.* water molecules, dissolved and suspended matter. Information about the environment is contained in the small part of the upwelling light transmitted through the surface (Novo *et al.*, 1989).

The radiant energy at wavelength λ , which emerges from the sea and constitutes the marine signal, originates from an upper layer whose thickness varies with λ . For remote sensing purposes, Gordon and McCluney (1975) have defined the penetration depth of light at wavelength $\lambda - z_{90}(\lambda)$. It is the thickness of the surface layer contributing 90% of the radiant energy observed just above the sea surface (excluding light directly reflected at the surface). Using a quasi-single scattering approximation, they found that the penetration depth $z_{90}(\lambda)$ does not differ significantly for different directions of radiation and is equal to the reciprocal of the diffuse attenuation coefficient for downwelling irradiance measured just below the sea surface:

$$z_{90}(\lambda) = [K_d(\lambda, z = 0)]^{-1}. \quad (1)$$

This equation was obtained on the assumption that the sea is optically homogeneous, infinitely deep and flat. In the case of optically stratified waters, the penetration depth can be calculated from the integral equation

$$\int_0^{z_{90}(\lambda)} K_d(\lambda, z) dz = 1. \quad (2)$$

The sensor receives the radiance L_s emerging from the sea surface layer that has been attenuated in travelling upwards from the surface to the sensor and modified by the radiance reflected at the rough sea surface and the atmospheric radiance (Austin, 1974):

$$L_s = T(L_w + L_r) + L_d, \quad (3)$$

where

L_w – underwater radiance transmitted through the water-air interface,

L_r – radiance reflected at the sea surface,

L_d – atmospheric radiance,

T – atmospheric transmittance of radiance from surface to sensor. All of these parameters depend on the wavelength λ .

Since upwelling radiation depends to a high degree on current irradiance conditions, in practice, in view of research into the relationships between optical properties and the remotely measured signal, L_w values are replaced by the reflectance. The reflectance at the water surface is defined as the ratio of upwelling irradiance $E_u(z)$ to downwelling irradiance $E_d(z)$, measured just above the sea surface ($z = 0$ m)

$$R = \frac{E_u(z)}{E_d(z)}. \quad (4)$$

The reflectance includes information on the optical properties of the water body (Smith, 1974) and can be evaluated from the remotely sensed radiance L_s using eq. (3). Values of $R(\lambda)$ are determined from satellite data from the relationship

$$R(\lambda) = \frac{Q \times L_w(\lambda)}{E_d(\lambda)}, \quad (5)$$

where Q – a constant of proportionality equal to π if the upwelling radiance is assumed to be isotropic. In calculations one usually takes $Q = \pi$, but if L_w is the radiance in the nadir direction, π must be replaced by a factor closer to 5 (Gordon and Morel, 1983).

Several methods of solving the radiative transfer equation that show the relationships between reflectance and the optical properties of the water yield similar results (Gordon and Brown, 1973; Gordon *et al.*, 1975; Jain and Miller, 1977; Morel and Prieur, 1977; Philpot, 1987; Whitlock *et al.*, 1981). Gordon *et al.* (1975) obtained the equation

$$R(\lambda) = \frac{0.33 b_b(\lambda)}{a(\lambda) + b_b(\lambda)}, \quad (6)$$

where b_b and a are the backscattering and absorption coefficients respectively.

Since absorption and scattering are additive, both a and b_b can be expressed as the sum of composite parts indicating the contribution of individual substances to these processes (Dera, 1992):

$$a(\lambda) = a_w(\lambda) + a_d^*(\lambda)n_d + a_p^*(\lambda)n_p + a_s^*(\lambda)n_s, \quad (7)$$

$$b_b(\lambda) = b_{bw}(\lambda) + b_{bs}^*(\lambda)n_s, \quad (8)$$

where n – concentration expressed in $[\text{mg m}^{-3}]$, * denotes the specific absorption or backscattering coefficient expressed in $[\text{m}^{-1} (\text{mg m}^{-3})^{-1}] \hat{=} [\text{m}^2 \text{mg}^{-1}]$, and subscripts w, d, p, s denote water, dissolved pigments, particulate organic pigments (chlorophyll), sediment and inorganic pigments respectively.

Water molecules absorb strongly at longer wavelengths and scatter at shorter wavelengths (Fig. 1). For sediment, absorption depends on several factors, particularly on its composition. Iron oxide compounds in the sediment absorb blue and violet light much like dissolved organic pigments (DOP). The strong absorption by water at longer wavelengths means that clear water will have a negligible reflectance in red and near-IR light. In estuaries and coastal water, reflectance is usually dominated by the suspended sediment, producing maximum reflectance between 550 and 650 nm. In the case of extremely high sediment loads ($>200 \text{ mg dm}^{-3}$), the maximum reflectance shifts into the red (650–700 nm) and even the near-IR ($>700 \text{ nm}$) band. This suggests an opportunity to apply ‘unmarine’ spectral ranges such

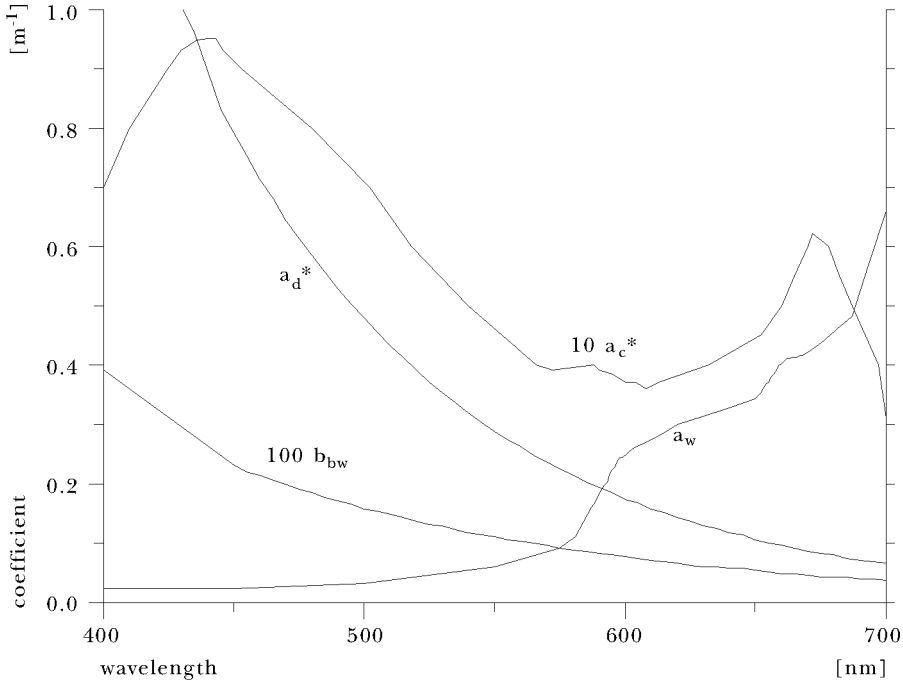


Fig. 1. Absorption and backscattering coefficients for water (a_w i b_{bw}), chlorophyll (a_c^*) and dissolved pigments (a_d^*)

as those from AVHRR channels 1 and 2 in the remote sensing of the seston content in water. Calculations have shown the generalised relationship between R and n_s to be

$$R = m \log(n_s) + l, \quad (9)$$

where m and l are regression constants (Stumpf, 1987). The application of similar empirical relationships in different parts of the ocean and in theoretical investigations has been presented, for example, by Albanakis (1990), Tassan and Sturm (1986) and Topliss *et al.* (1990).

In water with increased amounts of suspended matter, all backscattering can be considered as resulting from sediment only ($b_b = b_{bs}$), and absorption can be separated into absorption due to water, pigments and sediments. Then eq. (6) can be rewritten as

$$R(\lambda) = \frac{0.33 b_{bs}^*(\lambda)}{s^*(\lambda) + \frac{a_x(\lambda)}{n_s}}, \quad (10)$$

where $s^* = a_s^* + b_{bs}^*$ indicates the influence of sediment and $a_x = a_w + a_d^* n_d + a_p^* n_p$ the influence of water and organic pigments. For red and

near-IR light $a_x > 1 \text{ m}^{-1}$ and s^* is between 0.01 and 0.1 m^{-1} (Stumpf, 1987).

Using remote sensing, Spitzer *et al.*, (1990) estimated (from the AVHRR data) the suspended matter concentration in the North Sea to within 2–3 mg dm^{-3} . Gitelson and Kondratiev (1991) have shown that the estimation of seston concentration could have a standard deviation of less than 4 mg dm^{-3} .

3. Vertical distribution of suspended matter concentration in the southern Baltic

The vertical distribution of particles in seawater depends on a number of hydrophysical and biological factors in the sea. In general, their maximum concentration can be observed at the surface and in the layer just above the pycnocline. Below this, sinking particles are exposed to degradation (atrophy, oxidation, solution). An increase in seston concentration has also been observed near the bottom; this is caused by the floating of bottom sediments (Zalewski, 1973).

The density stratification, the result of the real distribution of temperature and salinity, limits the sinking of suspended matter through the pycnocline down to the bottom. In the deep-water zone, the variability of seston content is small during the whole year and mean values of this content range from 1.0 to 3.5 mg dm^{-3} . In Baltic waters, the subsurface and near-bottom zones are usually less transparent than intermediate waters:¹ the profiles in Figs. 2a and 2c show this very clearly and can be treated as typical of the Baltic Sea (Sagan, 1992).

Vertical distributions of suspended matter concentration differ in various regions and are strongly time-dependent. However, this variability is much smaller than their spatial variability. One feature characteristic of all profiles is that there is a relatively high particle content in the subsurface layer. In coastal waters two types of vertical seston concentration distribution prevail: one which is homogeneous uniform (Fig. 2b) and one with a subsurface layer of water rich in suspended matter. The mean concentration in the surface layer is about 5 mg dm^{-3} . The thickness of the layer

¹Suspended matter in water strongly influences the total light attenuation coefficient $c(\lambda)$. In the Gulf of Gdańsk the relationship between the suspended material concentration C [mg dm^{-3}] and the total attenuation coefficient measured at $\lambda = 535 \text{ nm}$ – $c(535)$ has been derived from

$$C = 2.95 \exp[0.335 c(535)] \quad [\text{mg dm}^{-3}]. \quad (11)$$

The variability of the total attenuation coefficient in the Gulf of Gdańsk and southern Baltic waters has been presented in sufficient detail in: Krężel and Sagan (1987), Sagan (1992), and the seston content in Krężel and Cyberski (1993).

with reduced transparency usually overlaps the pycnocline depth (Kreżel and Sagan, 1987).

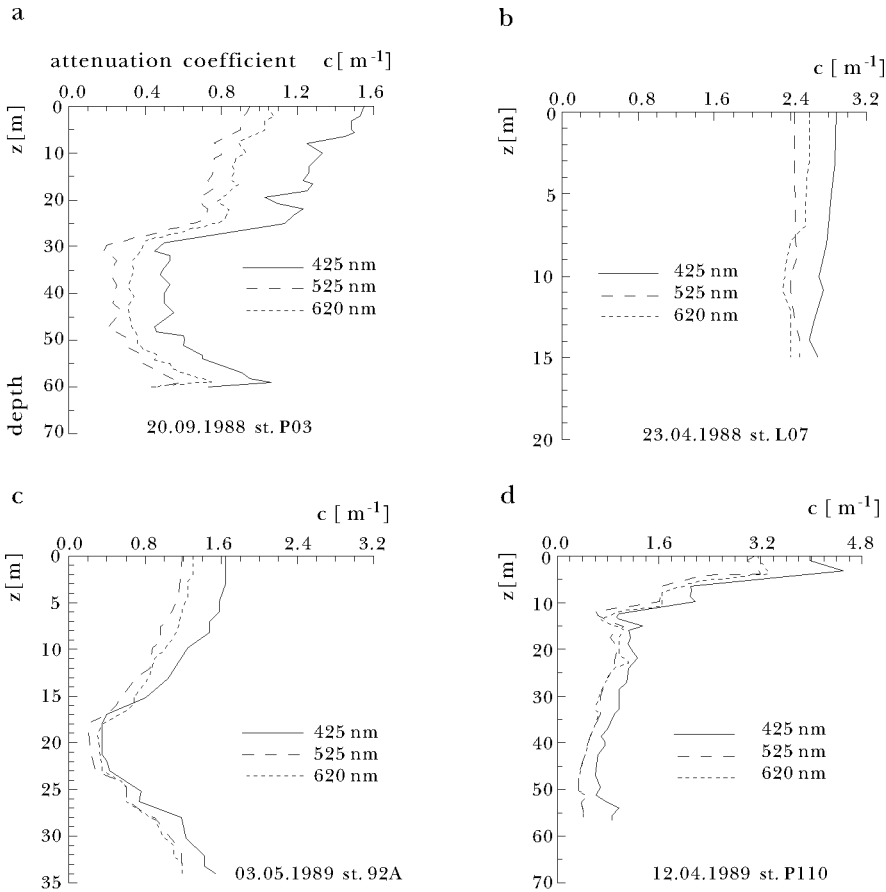


Fig. 2. Examples of the vertical distribution of the attenuation coefficient $c(\lambda)$ in Baltic waters (Sagan, 1992)

4. Methods

The remote sensing of the reflectance $R_s(\lambda)$ that would be measured just above the sea surface ($z = 0$ m) with various vertical profiles of seston content under the water transparency conditions of the Gulf of Gdańsk were simulated. This was done using Gordon and Clark's (1980) optical model with a light wavelength of 620 nm that here represents AVHRR channel 1 (580–680 nm). One reason for choosing 620 nm was that the characteristics of Baltic optical properties are frequently quoted for this

particular wavelength in the literature. The analysis was performed for two kinds of vertical seston concentration profiles:

- real profiles computed using green-light beam attenuation coefficients $c(535)$ measured *in situ*,
- modelled profiles with maximum surface concentration, including extreme situations where concentrations are very high.

The inherent and apparent optical properties for all profiles were computed from mathematical relationships available in the literature or derived from experimental data presented by a number of workers.

4.1. Optical model

Following Gordon and Clark (1980), a good estimation of the reflectance $R_s(\lambda)$ at the surface of stratified water is given by the relationship

$$R_s(\lambda) = p[X_s(\lambda)], \quad (12)$$

where p is a polynomial function², $X_s(\lambda)$ is a weighted, average function of the optical properties given by

$$X_s(\lambda) = \frac{\int_0^{z_{90}(\lambda)} X(\lambda, z) g(\lambda, z) dz}{\int_0^{z_{90}(\lambda)} g(\lambda, z) dz}, \quad (13)$$

where $X(\lambda, z)$ is a function of the inherent optical properties of seawater (André, 1992)

$$X(\lambda, z) = \frac{\frac{b_b}{a}}{1 + \frac{b_b}{a}}. \quad (14)$$

The contribution of a given layer to the water-leaving radiance that is a decreasing function of its depth is expressed by the weighting function:

$$g(\lambda, z') = \exp[-2 \int_0^{z'} K_d(\lambda, z) dz], \quad (15)$$

where

z' – depth of the elementary layer contributing to the light attenuation process.

4.2. Optically weighted concentration

The optically weighted concentration $C_{ef}(\lambda)$ is the concentration of suspended matter in a homogeneous water column from which the effective signal at wavelength λ would be the same as from a nonuniform profile

²According to Gordon *et al.* (1975), from Monte Carlo simulations:
 $p(x) = 0.001 + 0.3244x + 0.1425x^2 + 0.1308x^3$.

of concentration $C(z)$ (Gordon and Clark, 1980). The optically weighted concentration is obtained from the pigment profile in accordance with

$$C_{ef}(\lambda) = \frac{\int_0^{z_{90}(\lambda)} C(z) g(\lambda, z) dz}{\int_0^{z_{90}(\lambda)} g(\lambda, z) dz}, \quad (16)$$

where $g(\lambda, z)$ is the function defined previously (eq. 15). Gordon and Clark (1980) proposed to compare *in situ* measurements with satellite estimates by means of $C_{ef}(\lambda)$ computed from these measurements.

4.3. Optical properties

The total beam attenuation coefficient $c(\lambda)$

Eq. (11) can be rewritten as

$$c(535) = 2.98 \ln(C[\text{mg dm}^{-3}]) - 3.23. \quad (17)$$

In the absence of a similar relationship for southern Baltic waters, calculations in this region were also done using the above equation.

The close relationship between values of $c(\lambda)$ over the whole spectral range of visible light (Sagan, 1992) yields

$$c(620) = 0.971 c(535) + 0.198, \quad (18)$$

from experimental data and statistical descriptions presented by Woźniak *et al.* (1977), Olszewski *et al.* (1992) and Sagan (1992).

The absorption coefficient $a(\lambda)$

In the range of wavelengths $400 < \lambda < 550$ nm, the spectrum of absorption coefficients $a(\lambda)$ can be approximated with good accuracy by exponential functions in the form

$$a(\lambda) = a_w(\lambda) + \text{const} \times \exp(-\lambda\alpha), \quad (19)$$

where a_w – absorption coefficient for pure seawater, and α describes the slope of the absorption spectrum for the content of organic matter in water on a semi-logarithmic scale (Czyszek *et al.*, 1979; Woźniak, 1977; Woźniak *et al.*, 1977):

$$\alpha = \ln \frac{[a - a_w]_{\lambda_1}}{[a - a_w]_{\lambda_2}} \quad [\text{n m}^{-1}], \quad (20)$$

where $[a - a_w]\lambda = a(\lambda) - a_w(\lambda)$.

Since the role of water absorption in the process of light attenuation becomes ever more significant as the wavelength increases to over 550 nm, eq. (19) can be extended to the whole visible range of wavelengths, *i.e.*

400–700 nm (Wensierski, 1983). The constants obtained from measurements of $\lambda_1 = 450$ nm and $\lambda_2 = 550$ nm yield

$$a(\lambda) = a_w(\lambda) + [a - a_w]_{450} \exp[-\alpha(\lambda - 450)]. \quad (21)$$

In further calculations, $a(450)$ and $a(550)$ were assumed to be the average absorption coefficients in the surface layer of Baltic waters equal to 0.35 and 0.18 m^{-1} respectively (Woźniak, 1977). The absorption coefficients of pure water, according to Morel and Prieur (1977), are given as $a_w(450) = 0.015 \text{ m}^{-1}$, $a_w(550) = 0.064 \text{ m}^{-1}$ and $a_w(620) = 0.287 \text{ m}^{-1}$. The coefficient α calculated from eq. (20) is equal to $10.6 \times 10^{-3} \text{ nm}^{-1}$.

The average absorption coefficient $a(620)$, calculated from eq. (21), is 0.34 m^{-1} and falls into the range of average values of $a(620)$ characteristic of Baltic waters, where $a(620) = 0.35 \pm 0.11 \text{ m}^{-1}$ (Dera and Sagan, 1990). Taking into account the important role of water molecules in light absorption at 620 nm and the nonabsorbing properties of suspended matter at this wavelength (Dera, 1992; Wensierski, 1983; Woźniak, 1977), $a(620)$ in our analysis was assumed uniform from the surface to the penetration depth for all profiles examined:

The backscattering coefficient b_b

The volume backscattering coefficient can be approximately derived from (Dera, 1992)

$$\frac{b_b}{b} = \frac{1 - \frac{x_1}{3}}{2}, \quad (22)$$

where x_1 is the so-called elongation parameter. There is no significant difference between its values in the Gulf of Gdańsk and in Baltic waters generally and, in fact, does not depend on the light wavelength. Its value has been calculated at 2.88 (Woźniak, 1977). Thus the contribution of backscattering in the overall scattering was assumed to be

$$b_b(\lambda, z) = 0.02 b(\lambda, z). \quad (23)$$

The diffuse attenuation coefficient $K_d(\lambda)$

the experimental data allow statistical relationships to be derived between the diffuse attenuation coefficient $K_d(535 \text{ nm})$ and suspended matter concentration (Dera *et al.*, 1972).

$$K_d(535) = 0.0693 + 0.1026 C - 0.0017 C^2, \quad (24)$$

where C is the average concentration of suspended matter in the surface layer to a depth of 10 m expressed in $[\text{mg m}^{-3}]$, and calculated K_d is the average coefficient in this layer. $K_d(620)$ depends on $K_d(535)$ according to

$$K_d(620) = 0.266 + 0.638 K_d(535). \quad (25)$$

The above relationship was derived from average values of $K_d(\lambda)$ measured in the Baltic in 1972–1984 (Hapter, 1984; Koblentz-Mishke, 1987; Koblentz-Mishke *et al.*, 1985).

4.4. Profiles

Real profiles

98 vertical distributions of suspended matter concentration were examined. Concentration was calculated using eq. (11) with values of $c(535)$ measured in the Gulf of Gdańsk and open Baltic waters in 1985–1991 (Fig. 3).

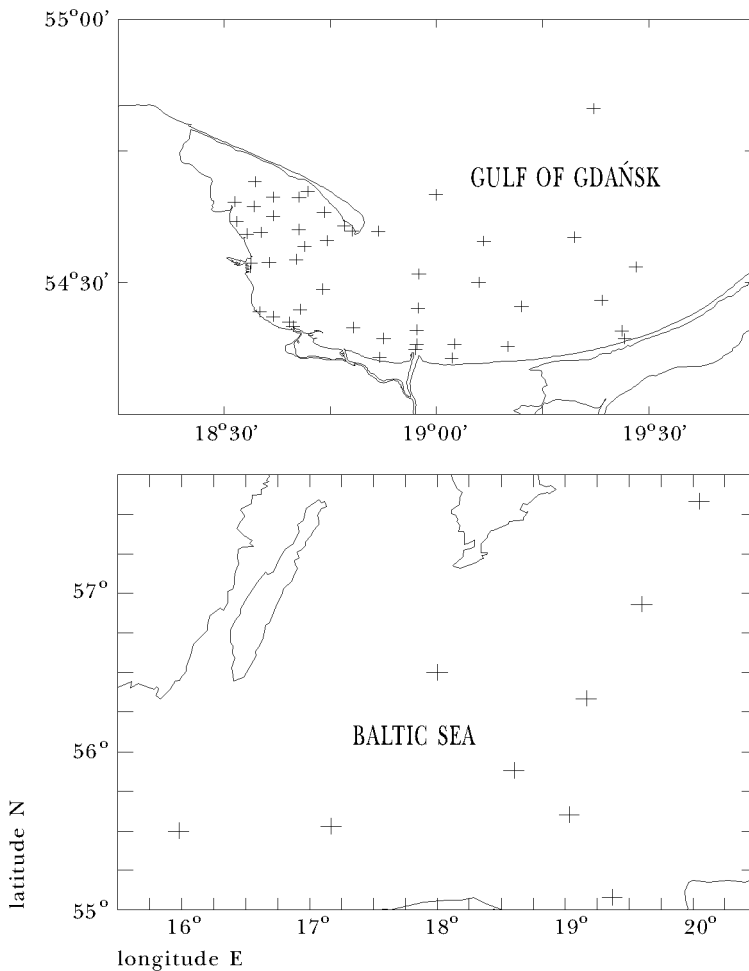


Fig. 3. Stations from which data were used in this paper

Calculations were done at least every 1 m down to a depth of 10 m and more frequently if it was possible. In the absence of measurements of $c(535)$ every 1 m, its values were linearly interpolated. At stations shallower than 10 m, the concentration was calculated to the bottom.

The concentration of suspended matter in the calculated profiles ranged from 3 to 27 mg dm^{-3} . The highest values were observed in summer, at depths of 0–6 m, but mostly at or just below the surface (to a depth of 2 m). Fig. 4 shows histograms of concentrations at the sea surface during various seasons. The year was divided into four seasons (Krężel and Sagan, 1987).

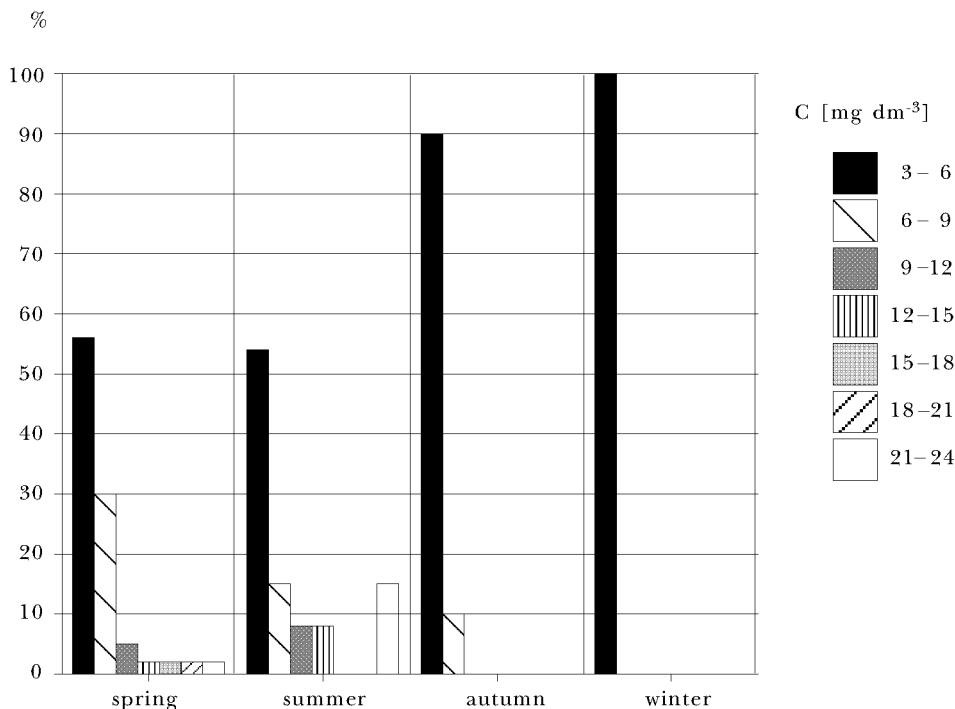


Fig. 4. Frequency distribution of surface concentration C [mg dm^{-3}] for the profiles in successive seasons

Amounts of suspended matter over 9 mg dm^{-3} (maximum 27.3 mg dm^{-3}) were recorded only near the Vistula river mouth in spring and summer, and in summer such values were noted in about 30% of profiles. Somewhat smaller values, *i.e.* 6–9 mg dm^{-3} , were present in this region in autumn and near smaller sources of seston such as the port in Gdynia, the sewage collector at Mechelinki and the Reda river during the whole year except winter.

In winter, suspended matter concentrations in all profiles did not exceed 6 mg dm^{-3} . In the open Baltic water this concentration was nearly 3 mg dm^{-3} except in summer when it increased to 6 mg dm^{-3} . Overall, about 70% of profiles examined had surface concentrations of less than 6 mg dm^{-3} . The average suspended matter concentration in vertical profiles varied from 3 mg dm^{-3} in the open Baltic to 20 in the Vistula mouth, but in most events (over 60%), it never exceeded 5 mg dm^{-3} . Nonuniform vertical seston profiles encompassed situations from nearly uniform with a standard deviation of 0.01–0.09 to markedly nonuniform with a maximum standard deviation of 7.55 mg dm^{-3} (Fig. 5). The maximum absolute concentration gradients in the surface layer were $3\text{--}13 \text{ mg dm}^{-3}/\text{m}$ and were mostly negative.

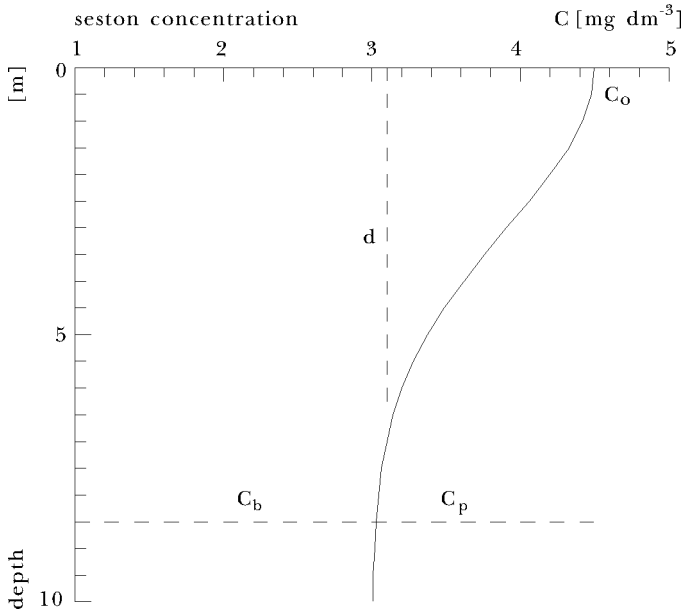


Fig. 5. Function of the vertical distribution of suspended matter $C(z)$ typical of the Baltic

Modelled profiles

In order to examine the influence of vertical stratification on satellite-estimated concentrations over a broad range of conditions, simulations were also done for designed profiles. The function given by

$$C(z) = C_b + (C_0 - C_b) \exp\left[-4.5\left(\frac{z}{d}\right)^2\right], \quad (26)$$

was assumed to be a reasonable imitation of a natural profile, where C_0 – surface concentration of suspended matter,

C_b – background concentration,

d – maximum concentration peak thickness.

Function $C(z)$ with parameter values typical of the region in question is shown in Fig. 5.

This function approximates cases where concentration is maximum at the surface and decreases continuously with depth. In the real profiles examined (described previously), maximum concentrations were also observed below the surface, but, in over 70% of events $C_{\max} = C_0$.

Profiles measured in these regions can be modelled using eq. (26) with the parameters in the ranges: $C_0(3, 30)$ [mg dm^{-3}], $C_b(1, 15)$ [mg dm^{-3}], $d(1, 50)$ [m]. Analysis of the frequency of these values in real profiles enabled a typical profile to be selected with the following parameter values: $C_0 = 4.5$ mg dm^{-3} (over 70% of surface concentrations were from 3 to 6 mg dm^{-3}), $C_b = 3.0$ mg dm^{-3} and $d = 9.0$ m (*ca.* 88% of values in the 1 – 5 mg dm^{-3} range and 68% in the 4 – 14 m range respectively). About 40% of the profiles examined were typical (parameter values within the above ranges).

From among the possible combinations of the parameter values of function $C(z)$ three profile types were selected (Fig. 6). They were classified according to the value of parameter A defined as the ratio of peak height above the background ($C_p = C_0 - C_b$) to its thickness and background concentration:

$$A = \frac{C_p}{d \times C_b}. \quad (27)$$

The ratio C_p/d characterises the mean gradient of the suspended matter concentration in the peak. Profiles for which $A < 0.01$ were taken to be type I; they were smooth and nearly uniform. Type II corresponded to the profiles with a visible concentration maximum that decreased slightly with increasing depth ($0.01 < A < 0.10$). Type III – sharp – contained seston distributions with marked concentration maxima and high gradients in the peak ($A > 0.1$).

By comparing modelled profiles, real profiles and the distribution of optical properties in the Baltic waters available in the literature (Krężel, 1980; Krężel and Cyberski, 1993; Krężel and Sagan, 1987; Sagan, 1992; Woźniak, 1977; Woźniak *et al.*, 1977), regions of frequent appearance each of these profile types were found.

Smooth profiles were the largest group (> 50%) among those examined. They were noted in turbid waters close to land-material sources as well as in open Baltic waters during the whole year. Their characteristic parameters were C_0 and $C_b < 6$ mg dm^{-3} and $d > 4$ m (mostly, however $d > 8$ m).

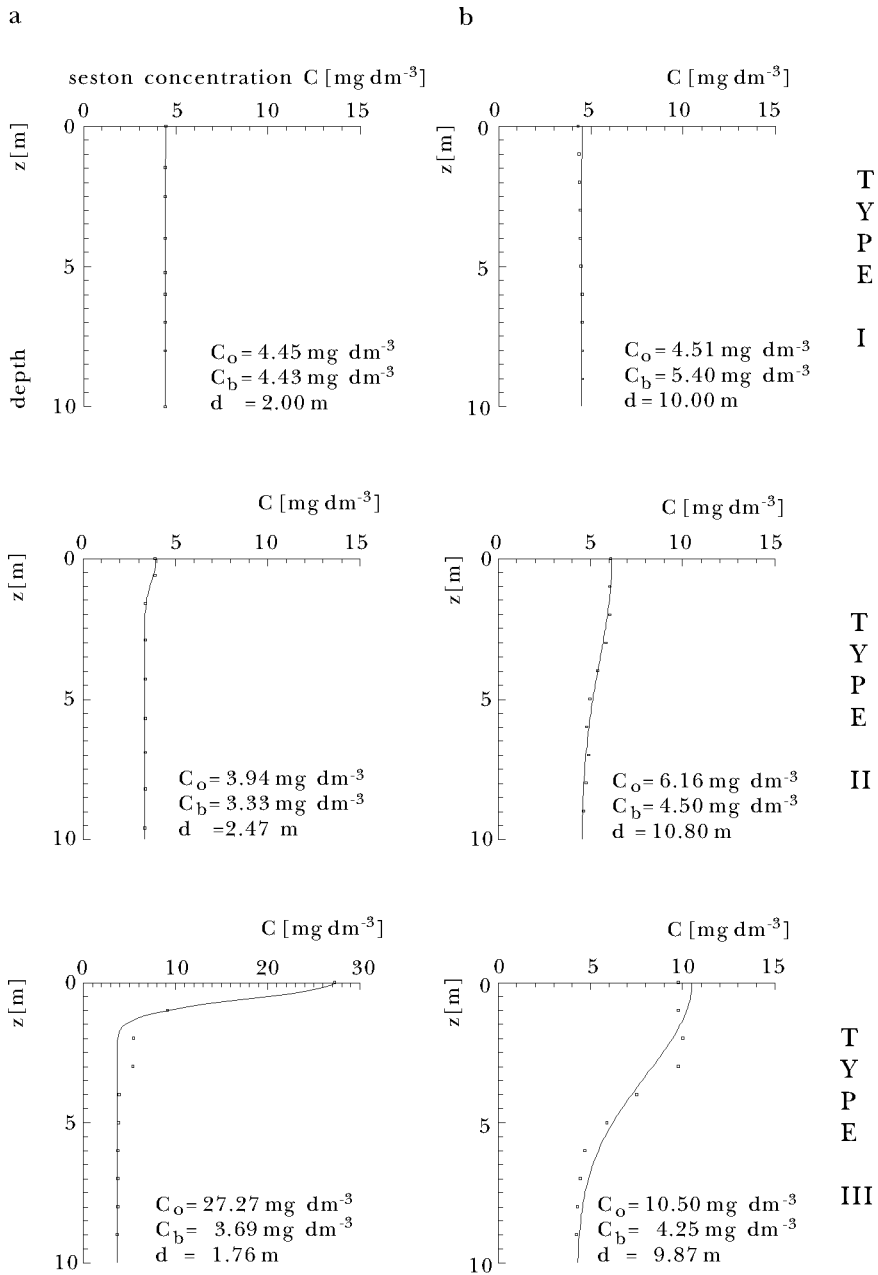


Fig. 6. Examples of agreement between real distributions and three modelled profiles of suspended matter for a thin layer (a) and a broad peak (b) of maximum concentration

Intermediate profiles – between smooth and sharp – occurred in every season at short distances from suspended matter sources (such profiles were noted in 34% of cases).

Type III profiles – sharp – were representative of typical profiles in the region of the largest flow of turbid waters, *i.e.* the Vistula river mouth, as well as at some distance from the mouth where source concentrations are high $C_0 > 8 \text{ mg dm}^{-3}$. Their peak thickness decreased with increasing distance from the source. Moreover, they were sometimes noted near smaller sources. Among the real profiles examined, sharp ones occurred in about 15% of events.

5. Calculations and results

The theoretical values of the reflectance $R_s(\lambda)$ that would be recorded by the radiometer just over the sea with given vertical distribution of seston $C(z)$ were calculated. To discover the influence of the inhomogeneity of this distribution on simulated reflectance values, the results were compared to R_h , R_0 i R_{ef} calculated for the profiles with constant seston concentration. Each of the investigated inhomogeneous vertical distributions of suspended matter (both theoretical and real) was compared with the three homogeneous profiles:

- concentration C_h , *i.e.* the mean seston concentration in a given profile down to the light penetration depth ($C_h = \langle C(z) \rangle_{z_0}$). Comparison of R_s and R_h yields information on the influence of profile inhomogeneity on the reflectance;
- concentration C_0 , *i.e.* the surface concentration of a given profile ($C_0 = C(z = 0 \text{ m})$). This enables one to find the conditions when subsurface changes in seston concentration exert no significant influence on the reflectance received over the sea surface ($R_s \approx R_0$);
- concentration equal to C_{ef} calculated for a given profile. Comparison of R_s and R_{ef} shows to what degree the optically-weighted concentration represents the real concentration deduced on the basis of reflectance measurements.

All the parameters used in the simulation are shown in Tab. 1.

Remotely sensed values of R_s , R_h , R_0 and R_{ef} were simulated according to Gordon and Clark's (1980) optical model (eqs. 12–15) for a light wavelength of 620 nm. The optical penetration depth was calculated using (1) for the values of $K_d(\lambda)$ obtained from eqs. (24) and (25) for inhomogeneous seston profiles. Coefficients $c(\lambda, z)$, $a(\lambda)$, $b_b(\lambda, z)$ were calculated for every kind of profile using eqs. (17–19). The optically weighted concentrations were calculated from eq. (16).

Table 1. Parameters used in the simulation

Symbol	Definition
Parameters of vertical seston distribution:	
C_0	seston concentration at the sea surface; $C_o = C(z = 0 \text{ m})$
C_b	'background' seston concentration
C_p	height of maximum seston concentration peak over background; $C_p = C_0 - C_b$
d	width of maximum seston concentration peak
Depths:	
$z_{90}(\lambda)$	optical penetration depth defined by Gordon and McCluney (1975)
Seston concentration in homogeneous profiles:	
C_h	arithmetic mean seston concentration down to optical penetration depth
C_{ef}	optically weighted concentration defined by Gordon and Clark (1980)
C_{sat}	seston concentration calculated from a comparison of simultaneously <i>in situ</i> measured seston and remotely measured reflectance
Reflectances:	
R_s	for an inhomogeneous seston profile
R_h	for a homogeneous seston profile with concentration C_h
R_0	for a homogeneous seston profile with concentration C_0
R_{ef}	for a homogeneous seston profile with concentration C_{ef}

The values of R_s and C_{ef} were calculated using Simpson's method with the error $E = 10^{-4}$. The smallest difference between two reflectances, capable of being detected by the radiometer ($\Delta R(620) = 0.001$), was obtained from eq. (5) by taking for AVHRR channel 1 the maximum measurable value, $E_d = 157 \text{ [mW cm}^{-2}\text{]}$ (Stumpf, 1987), and the radiometer sensitivity, $\Delta L = 0.052 \text{ [mW cm}^{-1} \text{ sr}^{-1}\text{]}$ (Gagliardini *et al.*, 1984).

5.1. Vertical seston concentration distributions (theoretically calculated)

5.1.1. The influence of vertical seston distribution parameters on remotely sensed optical properties of the water

The shape of the function $C(z)$ described by eq. (26) depends on the parameters of this function, *i.e.* C_0 , C_b and d . They characterise the

maximum and minimum seston concentrations and the width of its maximum concentration peak. The influence of these parameters on $R(620)$ was analysed, taking into account the typical vertical seston concentration profile (described in subsection 4.4.) with $C_0 = 4.5$, $C_b = 3.0 \text{ mg dm}^{-3}$ and $d = 9.0 \text{ m}$.

The influence of C_0

As can be seen in Fig. 7a, an increase in C_0 causes a significant increase in $R(\lambda)$ regardless of the profile shape (homogeneity). Within C_0 a range between 3 and 20 mg dm^{-3} , for $\Delta C_0 = 0.5 \text{ mg dm}^{-3}$, $\Delta R(\lambda) > 0.1\%$ increases. The increase in surface seston concentration causes the mean concentration in the whole profile to increase and, as a final result, the penetration depth z_{90} to decrease. This depth within whole range of C_0 is reduced to such an extent ($z_{90} < 2 \text{ m}$) that the seston profile shape has no significant influence on the upwelling radiance. Thus the reflectance $R(\lambda)$ reflects the surface concentration, which is close to C_h owing to the small penetration depth. The seston profile exerts its greatest influence on the surface reflectance (unrecorded by the radiometer) when $C_0 = 8 \text{ mg dm}^{-3}$. The differences $|R_s - R_0|$ and $|R_s - R_h|$ are equal to 0.08 and 0.06% respectively.

The influence of d

An increase in d smooths the maximum seston concentration peak and leads simultaneously to an increase in this concentration just under the sea surface. As a result, a larger mass of suspended matter takes part in creating the remotely sensed radiance. This can be seen in Fig. 7b as an increase in $R(\lambda)$ as d increases to 10 m. A further increase in d has no influence on $R(\lambda)$ because it does not cause the seston concentration within the layer penetrated by light ($C_h \approx C_0$) to change. Subsurface changes in the seston concentration, caused by the increase in peak width, have a significant influence on the radiance sensed by the radiometer. Differences $|R_s - R_0|$ are as high as $\approx 1.4\%$ for the smallest d and decrease with increasing peak width. The influence of the profile shape is not so great, but significant enough within the range of d from 1 to 6 m, where $|R_s - R_h| > 0.1\%$.

The influence of C_b

The increase in C_b up to $C_b = C_0$ causes a smoothing of the vertical seston concentration distribution, *i.e.* a decrease in the absolute vertical concentration gradients. Any further increase in C_b causes the absolute gradients to increase and function $C(z)$ becomes larger. An increase in this parameter causes the total seston concentration in the whole water column to increase, and as a result the penetration depth decreases from 2.2 to about 1 m. However, the increase in C_b has a minimal influence on seston

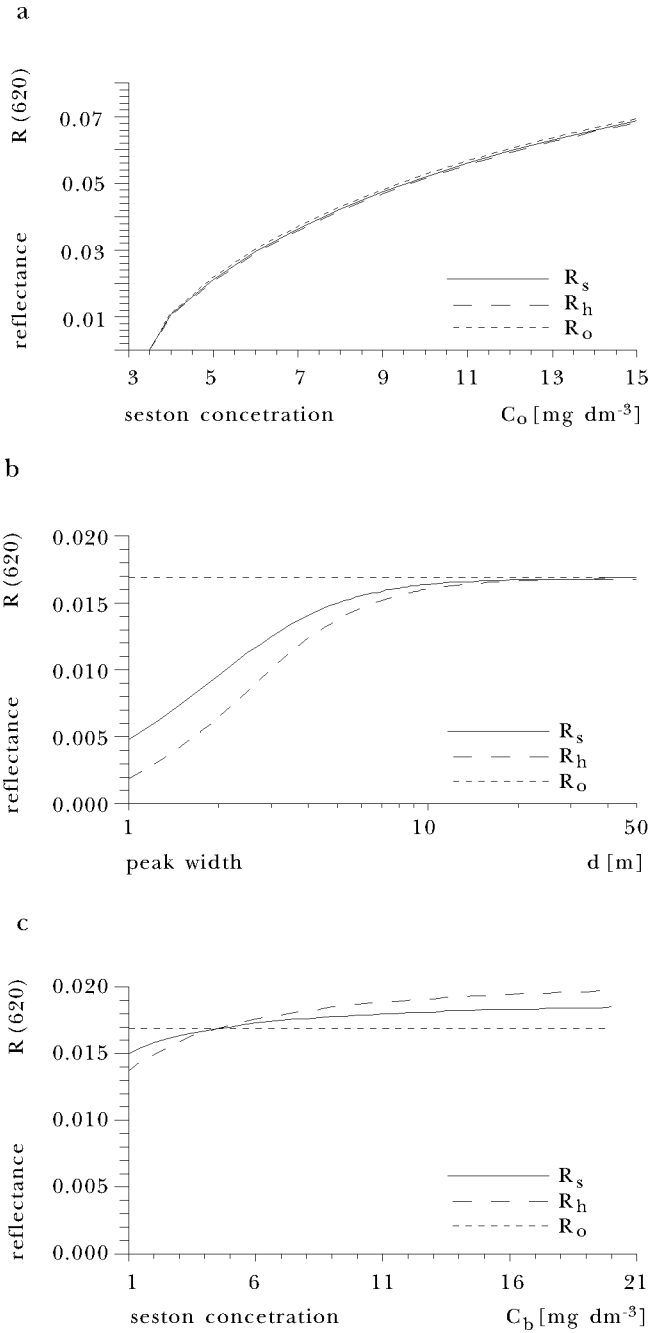


Fig. 7. Dependence of $R(620)$ on the parameters of the vertical seston distribution function, $C(z)$: surface concentration C_0 (a), peak width d (b), background concentration C_b (c)

concentration just under the sea surface and causes only a small increase in R_s with an increase in C_b up to 10 mg dm^{-3} (Fig. 7c). A further increase in C_b does not change the value of $R(\lambda)$ for homogenous or inhomogeneous seston profiles. The influence of the profile shape on remotely sensed reflectance is small but significant when $C_b < 2 \text{ mg dm}^{-3}$ and $C_b > 14 \text{ mg dm}^{-3}$, where $|R_s - R_h| > 0.1\%$. To equate the remotely sensed seston concentration and the surface concentration is possible only for a C_b range between 2.5 and 10 mg dm^{-3} where $|R_s - R_0|$ does not exceed 0.1%.

5.1.2. The influence of seston vertical distribution inhomogeneity on radiance sensed over the sea surface

The dependence of radiance measured by AVHRR on the inhomogeneity of vertical seston distribution for the three types of profile described in subsection 4.4 has been analysed. For the smooth (type I), intermediate (type II) and sharp (type III) profiles parameter A was assumed equal to 0.01, 0.05 and 0.10 respectively. The results of calculations are shown as dependences of $R(620)$ on the seston surface concentration and the width of its maximum concentration peak. The values of C_0 and d change within the range defined earlier.

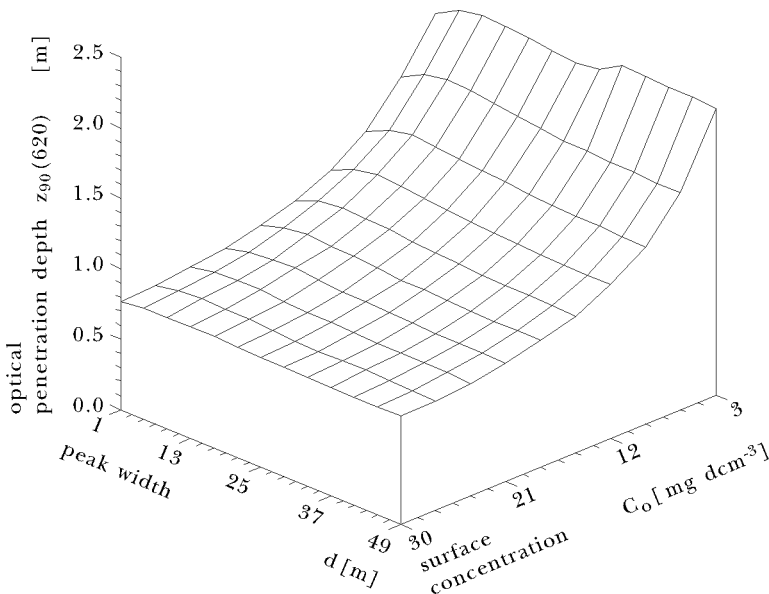


Fig. 8. Dependence of optical penetration depth $z_{90}(620)$ on surface concentration C_0 and peak width d for type II profiles

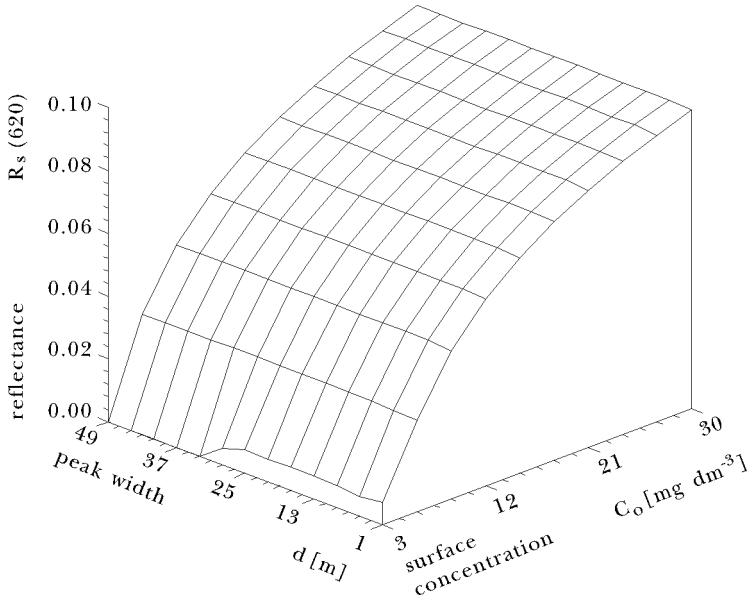


Fig. 9. Reflectance $R_s(620)$ vs. seston surface concentration C_0 and peak width d for type II profiles

In none of the analysed seston profiles does the optical penetration depth exceed 2.5 m. Values of $z_{90}(620)$ fall within 0.8–2.5 m. The variability of the penetration depth vs. C_0 and d , in type II profiles is shown in Fig. 8. The influence of the width of d on z_{90} is negligible except in profiles with low surface seston concentrations, where the influence of d on z_{90} is slight. Instead, there is a distinct dependence of the optical penetration depth on the surface concentration; z_{90} decreases exponentially with the increase in C_0 .

In spite of this reduction in optical penetration depth, the increase in total seston concentration in this layer, due to the increase in C_0 , causes the reflectance R_s to increase significantly and attains values of up to 0.09 for the largest C_0 (Fig. 9). For surface concentrations over 5 mg dm⁻³, the influence of the peak width on R_s is weak. The lowest values are for the surface concentration close to 3 mg dm⁻³.

The variability in $R_s - R_h$ and $R_0 - R_s$ vs. C_0 and d is shown in Fig. 10. For all profiles $R_s > R_h$, but in the majority of events the differences do not exceed 0.1% (0.2% at most). Differences between R_s and R_0 are greater and reach 0.3% with $R_0 > R_s$. Generally, when the peak broadens up to 3 m, the absolute differences between R_s and $R(620)$ simulated for the homogeneous profiles decrease, and their maximum values are recorded for the low surface concentrations.

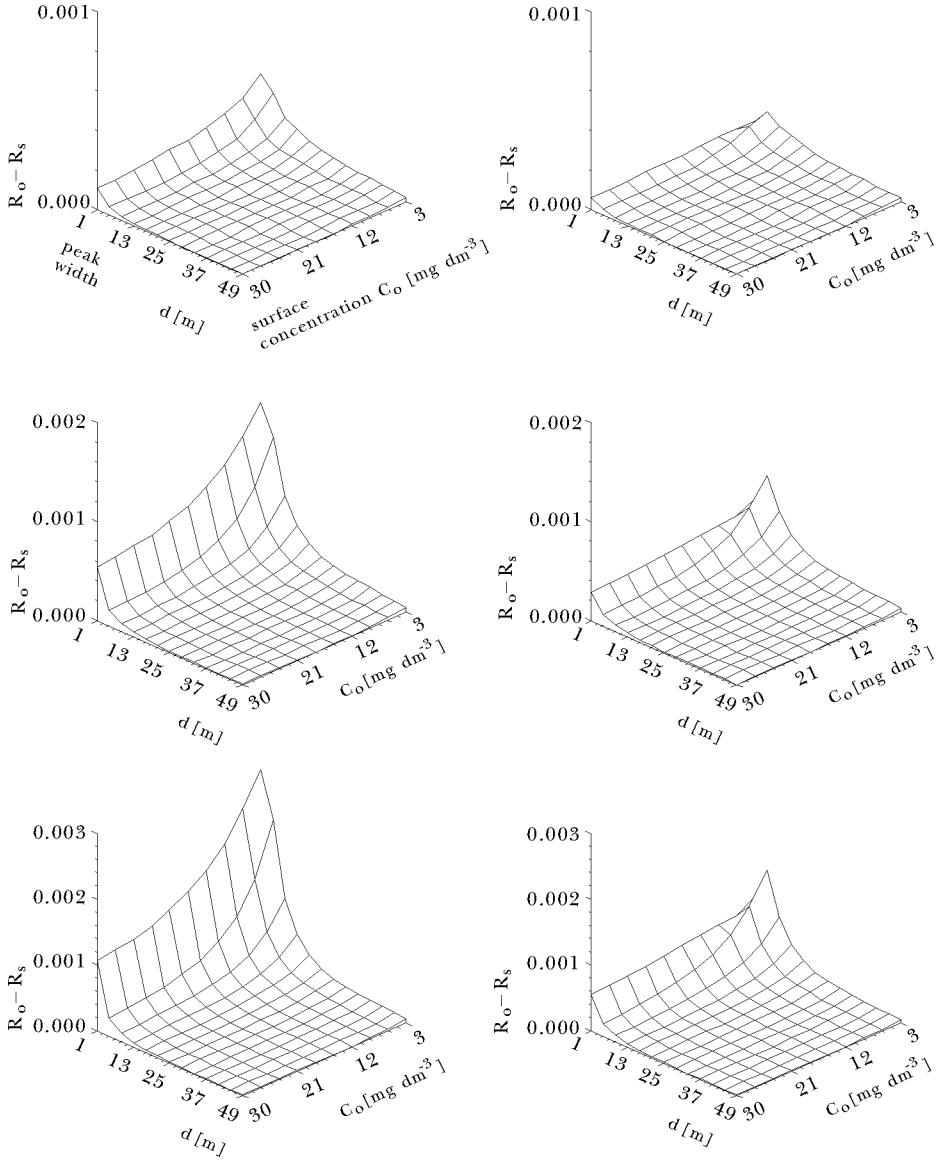


Fig. 10. Comparison of reflectance $R(620)$ calculated for inhomogeneous and homogeneous profiles with seston concentrations of C_h (a) and C_0 (b)

The inhomogeneity of vertical seston distribution on simulated radiance exerts the greatest influence on the sharp profiles (type III). Particularly large differences of $|R_s - R_h|$ were observed for profiles with surface concentrations below 8 mg dm^{-3} and a peak width below 3 m. There are no significant differences over the whole range of C_0 for this type of profile only

when $d > 5$ m or $d = 1$ m, and when $C_0 > 10$ mg dm⁻³. In the majority of type II and smooth profiles, the vertical distribution inhomogeneity has no significant influence on the value of $R(620)$, *i.e.* $R_s \approx R_h$. The value of the reflectance depends exclusively on the total mass of suspended matter in the light penetration layer.

Values of R_s and R_0 are similar in all cases of type I profiles. The subsurface variability of seston concentration on reflectance does, however, have a distinct influence on type II and III profiles, where $|R_0 - R_s|$ may reach 0.3%. In the case of intermediate and sharp profiles there are similar values of R_s and R_0 for $d > 5$ m and $d > 10$ m respectively within the whole range of C_0 . Significant differences between R_s and R_0 (up to 1%) occur for type III profiles with a very narrow maximum concentration width (< 3 m). This is the typical situation near the Vistula river mouth.

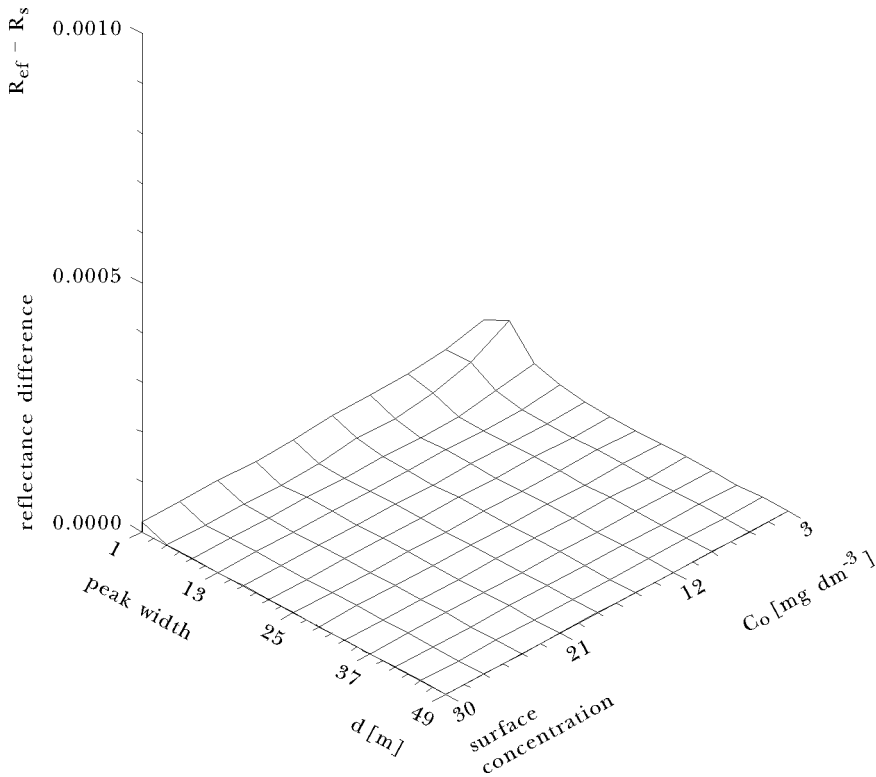


Fig. 11. Differences between the values of $R(620)$ calculated for inhomogeneous and homogeneous profiles with a seston concentration of E_{ef} . Results for the sharp profiles

Fig. 11 shows the results of comparing R_s with R_{ef} , *i.e.* simulated for homogeneous profiles with seston concentration C_{ef} . Slight differences between

R_s and R_{ef} occur only for distributions with low C_0 and small d (< 5 m); they never exceed 0.08%. For other distributions, according to Gordon and Clark's theory, $R_s = R_{ef}$.

5.2. Real seston distributions

The optical penetration depth $z_{90}(620)$ for the investigated profiles ranges between 0.88 (for an average concentration of C within the 10 m surface layer, $\langle C \rangle_{10} = 20 \text{ mg dm}^{-3}$) and 1.9 m ($\langle C \rangle_{10} = 3.3 \text{ mg dm}^{-3}$). The dependence of $z_{90}(620)$ on surface seston concentration C_0 is shown in Fig. 12.

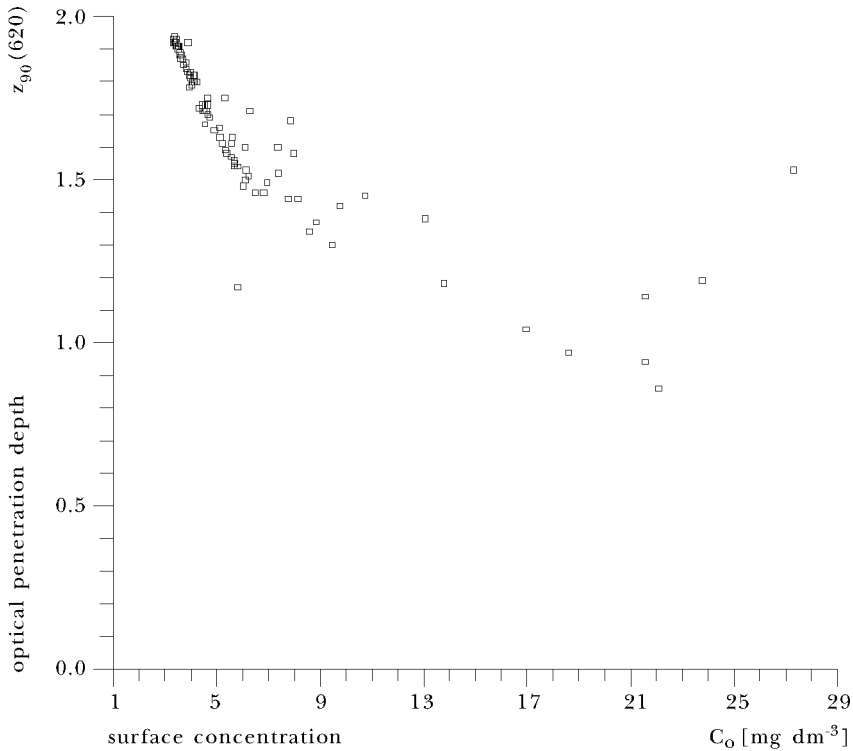


Fig. 12. Optical penetration depth for red light (620 nm) *vs.* seston concentration at the sea surface

The ratio of R_s values, calculated for real profiles, to the ones simulated for homogeneous distributions with the seston concentrations of C_h , C_0 and C_{ef} that would be measured just over the sea surface, *vs.* seston surface concentration is shown in Fig. 13. This shows clearly that seston concentration estimated on the basis of satellite data can be interpreted as the average

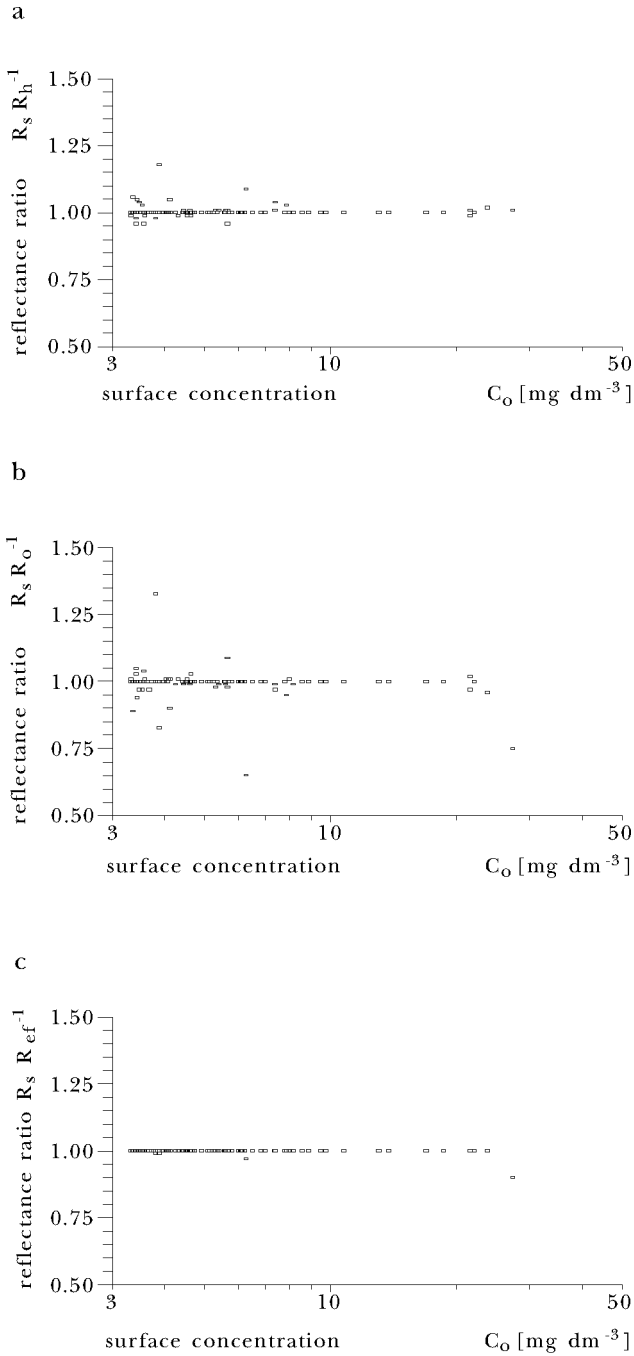


Fig. 13. Ratios of R_s calculated for real profiles to $R(620)$ for homogeneous profiles at seston concentrations of C_h , C_0 and C_{ef} vs. surface concentration C_0

concentration within the optical penetration layer. In 95% of investigated events the calculated values of R_h were equal to or differ insignificantly from R_s .

Absolute differences between the values of R_s and R_0 are more significant and for the profiles compared are as large as 2.3%. The greatest occur for the profiles with a steep gradient of C in the layer down to depth z_{90} . Differences between R_s and R_0 were recorded even for the highest values of C_0 and $\Delta C/\Delta z$. This means that the real values of C_0 occurring in the investigated area are still too low to dominate fully the upwelling radiance. Thus, the subsurface shape of the concentration profile cannot be ignored in the calculations.

The consistency R_s and R_{ef} (Fig. 13c) confirms the results obtained for theoretically assumed seston distributions discussed earlier.

6. Discussion

The influence of the vertical seston profile on the reflectance $R(620)$ just over the sea surface was analysed on the basis of theoretically assumed distributions of seston concentration. The distribution parameters C_0 , C_b and d were given values within the range characteristic of the Baltic.

The results shown in Fig. 10 clearly indicate that in the majority of events the influence of the seston vertical distribution shape on a remotely sensed signal is negligible. The considerable differences between R_s and R_h , leading to a rather doubtful estimate of average seston concentration within the optically penetrated layer on the basis of remotely sensed reflectance, occur only for type III profiles *i.e.* in the vicinity of the mouths of the Vistula river and smaller sources. This is confirmed by the analysis of real profiles analysis (Fig. 13a), where significant differences between R_s and R_h were observed in those areas. The insufficient quantity of field data makes statistical analysis of its characteristic features impossible. Using an algorithm constructed on the basis of a comparison of R_s and C_h will cause the seston concentration in those regions to be overestimated.

Comparison of Figs. 10a and 10b shows that consistency between R_s and R_0 occurs when $R_s \approx R_h$. This means that calculated C_{sat} is an estimate of surface suspended matter concentration C_0 when $C_0 \approx C_h$. The differences between R_s and R_0 for the same profiles were bigger than between R_s and R_h . The conclusion is that values of C_{sat} are closer to C_h than to C_0 . If $R_0 > R_s > R_h$, C_h cannot be equal to C_0 . For the real profiles investigated, a consistency between R_s and R_0 was observed when $|C_h - C_0| < 0.12 \text{ mg dm}^{-3}$. It is a comparatively small difference (as compared to the values of C_0).

The above considerations indicate that reflectance measured over sea level depends on the seston concentration not only at the surface itself but in the whole surface layer. Even high values of C_0 cannot dominate the upwelling radiance sufficiently to render subsurface variability of seston concentration insignificant to remotely sensed reflectance. Nevertheless, it is the surface seston concentration that plays the predominant role in creating the upwelling radiance (cf. Fig. 9). This has been confirmed by the high correlation (99.8%) between C_0 and R_s calculated for the real profiles. The estimated relationship can be written as

$$C(z = 0[m]) = 3.06 \exp(23.39 R_s). \quad (28)$$

84% of real values of C_0 differ from the values calculated using eq. (28) by less than $\pm 0.4 \text{ mg dm}^{-3}$ (Fig. 14).

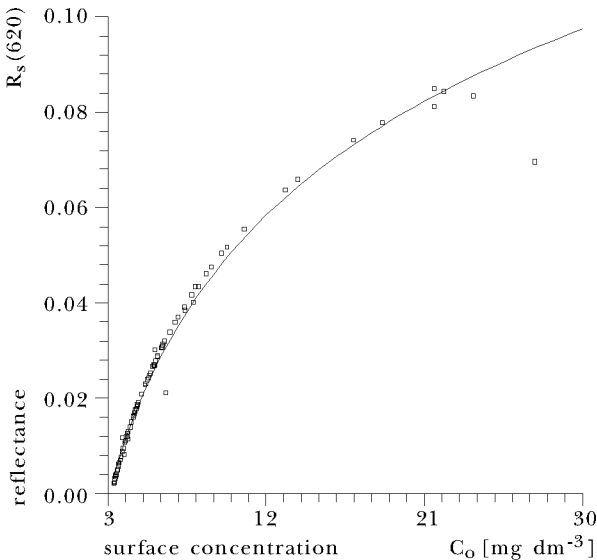


Fig. 14. Reflectance $R_s(620)$ vs. seston surface concentration in the Gulf of Gdańsk

According to eq. (28), the minimum increase in surface concentration C_0 causing a noticeable change in reflectance ($\Delta R > 0.1\%$) is 0.5 mg dm^{-3} for $C_0 < 20 \text{ mg dm}^{-3}$, and about 1 mg dm^{-3} for higher concentrations. Nevertheless, for the most frequent concentrations of C_0 , *i.e.* outside the Vistula river mouth ($C_0 < 8 \text{ mg dm}^{-3}$), a difference of about 0.25 mg dm^{-3} can cause a noticeable change in $R(620)$. An analysis of the influence of all $C(z)$ parameters on the reflectance $R(620)$ over the sea surface, for a typical vertical distribution of seston, leads to the conclusion that the minimum change in seston concentration that can be sensed remotely is about 0.5 mg dm^{-3} .

The high correlation between $R_s(620)$ and $C_h (= \langle C(z) \rangle_{z_0})$ observed for real profiles proves that the influence of its shape on R_s is negligible. The relationship (Fig. 15)

$$C_h = 3.09 \exp(22.52 R_s), \quad (29)$$

enables the mean value of seston concentration to be calculated within the optical penetration layer with an error of $\pm 1.85 \text{ mg dm}^{-3}$. But in about 90% of events this error did not exceed 0.3 mg dm^{-3} .

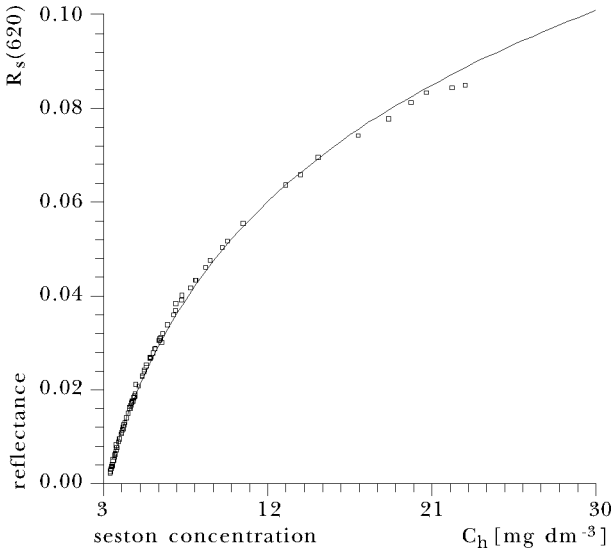


Fig. 15. Reflectance $R_s(620)$, vs. mean seston concentration in the optical penetration layer of the Gulf of Gdańsk

According to Gordon and Clark's theory, the remotely sensed seston concentration corresponds to the previously defined optically weighted concentration. The results of the analysis shown in Figs. 11 and 13c confirm that the homogeneous profile with a concentration of C_{ef} gives the same signal as the equivalent inhomogeneous one (with a concentration of $C(z)$). The dependence of C_{ef} on the surface concentration C_0 for various values of the parameters d and C_b of the $C(z)$ function is shown in Fig. 16.

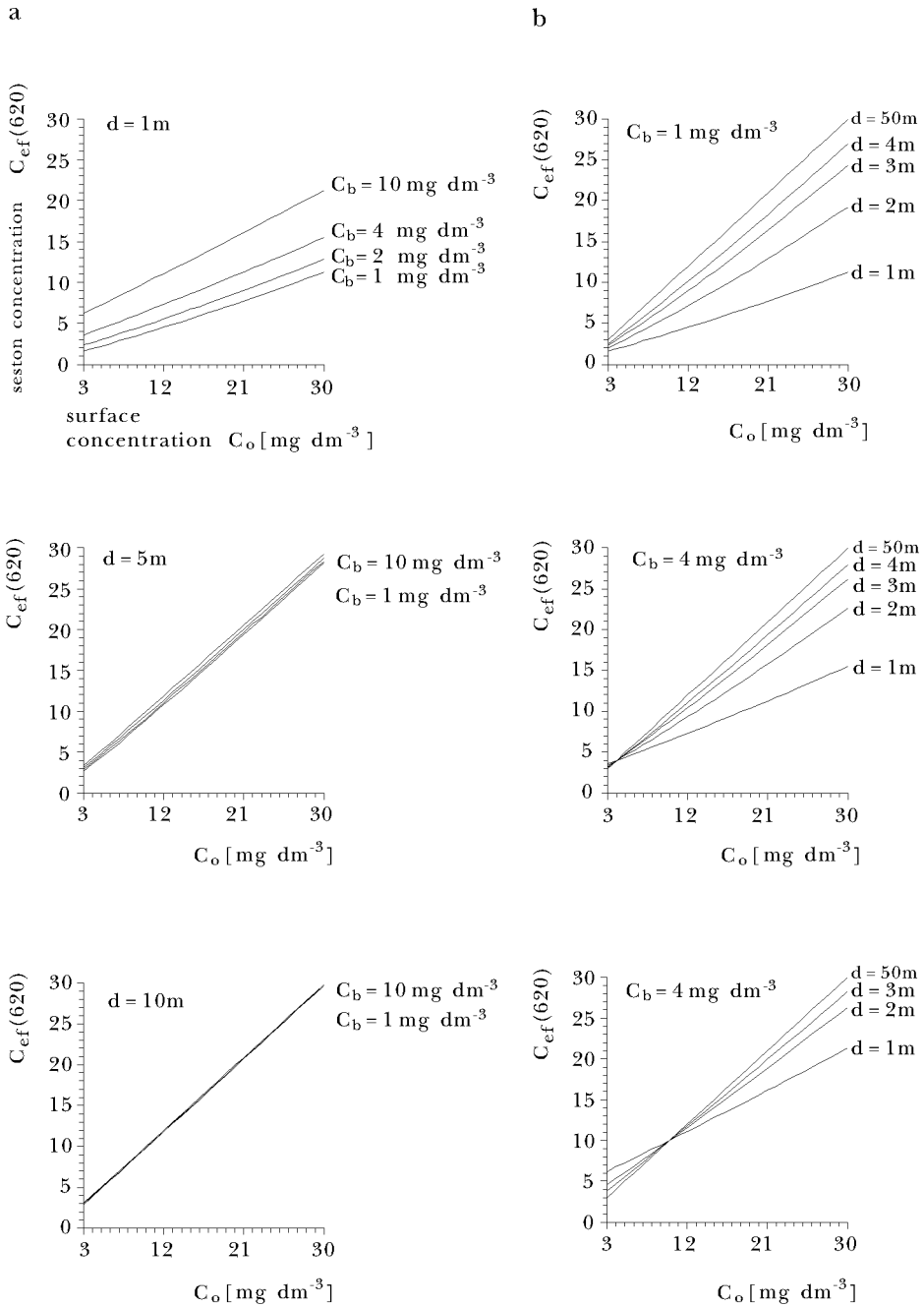


Fig. 16. Dependence of the optically weighted concentration C_{ef} on C_o for various values of background concentration when $d = \text{const}$ (a); maximum concentration peak width when $C_b = \text{const}$ (b)

7. Conclusions

- The vertical distribution of suspended matter in the investigated area has only a small influence on a remotely sensed signal. Only within regions where surface concentrations exceed 8 mg dm^{-3} and decrease rapidly with depth, can the assumption that $C_s = C_h$ lead to significant errors.
- The remotely sensed reflectance depends on the suspended matter concentration within the whole optical penetration layer. Remote estimation of surface concentration is possible only when $C_0 \approx C_h$. This condition is fulfilled for the majority of the southern Baltic vertical seston distributions, except in the Vistula river mouth area.
- According to Gordon and Clark's theory, the homogeneous vertical seston profile with a concentration equal to that calculated for an inhomogeneous profile yields a reflectance identical to the inhomogeneous one.
- It is possible to record surface seston concentration changes of the order of 1 mg dm^{-3} in the vicinity of the Vistula river mouth and of 0.5 mg dm^{-3} beyond it with remote sensing methods.

References

- Albanakis K. S., 1990, *Testing of a model for the simulation of the volume reflectance of water due to suspended sediment under controlled conditions, for various sediment types*, Int. J. Remote Sens., 11 (9), 1533–1547.
- André J. M., 1992, *Ocean color remote-sensing and the subsurface vertical structure of phytoplankton pigments*, Deep-Sea Res., 39, 763–779.
- Austin R. W., 1974, *The remote sensing of spectral radiance from below the ocean surface*, [in:] *Optical aspects of oceanography*, N. G. Jerlov and E. Steemann Nielsen (eds.), Academic Press, London, New York, 317–343.
- Czyszek W., Wensierski W., Dera J., 1979, *Solar radiation energy inflow and absorption in the Baltic water*, Stud. i Mater. Oceanol., 26, 105–141, (in Polish).
- Dera J., 1992, *Marine physics*, Elsevier, Amsterdam–Oxford–New York–Tokyo, 516 pp.
- Dera J., Sagan S., 1990, *A study of the Baltic water optical transparency*, Oceanologia, 28, 77–102.
- Dera J., Zalewski S. M., Zajwroniuk T., 1972, *Preliminary study of a correlation between attenuation of irradiance and the concentration of suspended matter in the sea*, Acta Geophys. Pol., 20, 3–4, 305.

- Gagliardini D. A., Karszenbaum H., Legeckis R., Klemas V., 1984, *Application of Landsat MSS, NOAA TIROS AVHRR, and Nimbus CZCS to study the La Plata River and its interaction with the ocean*, Remote Sens. Environ., 15, 21–36.
- Gitelson A. A., Kondratiev K. Ya., 1991, *Optical models of mesotrophic and eutrophic water bodies*, Int. J. Remote Sens., 12 (3), 373–383.
- Gordon H. R., 1978, *Remote sensing of optical properties in continuously stratified waters*, Appl. Opt., 17 (12), 1893–1897.
- Gordon H. R., Brown O. B., 1973, *Irradiance reflectivity of a flat ocean as a function of its optical properties*, Appl. Opt., 12 (7), 1549–1551.
- Gordon H. R., Brown O. B., 1975, *Diffuse reflectance of the ocean: some effects of vertical structure*, Appl. Opt., 14, 2892–2895.
- Gordon H. R., Brown O. B., Jacobs M. M., 1975, *Computed relationships between the inherent and apparent optical properties of a flat homogenous ocean*, Appl. Opt., 14, 417–427.
- Gordon H. R., Clark D. K., 1980, *Remote sensing optical properties of a stratified ocean: an improved interpretation*, Appl. Opt., 19, 3428–3430.
- Gordon H. R., McCluney W. R., 1975, *Estimation of the depth of sunlight penetration in the sea for remote sensing*, Appl. Opt., 14, 413–416.
- Gordon H. R., Morel A. Y., 1983, *Remote assessment of ocean color for interpretation of satellite visible imagery. A review*, Lecture Notes on Coastal and Estuarine Studies, 4, Springer-Verlag, New York–Berlin–Heidelberg–Tokyo, 114 pp.
- Hapter R., 1984, *Optical conditions of organic matter photosynthesis in the Baltic*, Ph. D. thesis, IO PAN, Sopot, (in Polish).
- Jain S. C., Miller J. R., 1977, *Algebraic expression for the diffuse irradiance reflectivity of water from the two-flow model*, Appl. Opt., 16, 202–204.
- Koblentz-Mishke O. I. (ed.), 1987, *Ekosistemy Baltiki v maye-iyune 1984 goda*, Akad. Nauk SSSR, Moskva, (in Russian).
- Koblentz-Mishke O. I., Woźniak B., Ochakowski Y. E., 1985, *Utilization of solar energy in the photosynthesis process of the Baltic and Black Seas phytoplankton*, P. P. Shirshov Institute of Oceanology of A. S. of USSR and Institute of Oceanology of RAS, Moskva, (in Russian).
- Krężel A., 1980, *Measurements of the total light attenuation coefficient in the Gulf of Gdańsk in 1975–1978*, Zesz. Nauk. BiNoZ UG, Oceanografia, 7, 25–40, (in Polish).
- Krężel A., Cyberski J., 1993, *Influence of the Vistula river on suspended matter content in the Gulf of Gdańsk waters*, Stud. i Mater. Oceanol., 64, 27–39.
- Krężel A., Sagan S., 1987, *Variability of the total light attenuation coefficient in water of the Gulf of Gdańsk*, Stud. i Mater. Oceanol., 51, 49–82, (in Polish).
- Morel A., Prieur L., 1977, *Analysis of variations in ocean color*, Limnol. Oceanogr., 22 (4), 709–722.

- Munday J. C., Alfoldi T. T., 1979, *Landsat test of diffuse reflectance models for aquatic suspended solids measurements*, Rem. Sens. Environ., 8, 169–183.
- Novo E. M. M., Hansom J. D., Curran P. J., 1989, *The effect of viewing geometry and wavelength on the relationship between reflectance and suspended sediment concentration*, Int. J. Remote Sens., 10 (8), 1357–1372.
- Olszewski J., Sagan S., Darecki M., 1992, *Spatial and temporal changes in some optical parameters in the southern Baltic*, Oceanologia, 33, 87–103.
- Pak H., Codispoti L. A., Zaneveld J. R. V., 1980, *On the intermediate particle maxima associated with oxygen-poor water off Western South America*, Deep-Sea Res., 27A, 783–797.
- Philpot W. D., 1987, *Radiative transfer in stratified waters: A single scattering approximation for irradiance*, Appl. Opt., 26 (19), 4123–4132.
- Ritchie J. C., Cooper C. M., Yongqing J., 1987, *Using Landsat multispectral scanner data to estimate suspended sediments in Moon Lake, Mississippi*, Rem. Sens. Environ., 23, 65–81.
- Robinson I. S., 1985, *Satellite oceanography*, Ellis Horwood Limited, Chichester, 455 pp.
- Sagan S., 1992, *Light transmission in the southern Baltic waters*, Rozprawy i monografie, 2, Inst. Oceanol. PAN, Sopot, 149 pp., (in Polish).
- Sathyendranath S., Platt T., 1989, *Remote sensing of ocean chlorophyll: consequence of nonuniform pigment profile*, Appl. Opt., 28, 490–495.
- Smith R. C., 1974, *Structure of solar radiation in the upper layers of the sea*, 5, [in:] *Optical aspects of oceanography*, N. G. Jerlov and E. Steemann Nielsen (eds.), Academic Press, London, New York, 95–119.
- Spitzer D., Laane R., Roozkrans J. N., 1990, *Pollution monitoring of the North Sea using NOAA AVHRR imagery*, Int. J. Remote Sens., 11 (6), 967–977.
- Stumpf R. P., 1987, *Application of AVHRR satellite data to the study of sediment and chlorophyll in turbid coastal water*, Tech. Memo. NESDIS AISC 7, Natl. Environ. Satell. Data, and Int. Serv., Natl. Oceanic and Atmos. Admin., Washington, D. C., 50.
- Tassan S., Sturm B., 1986, *An algorithm for the retrieval of sediment content in turbid coastal waters from CZCS data*, Int. J. Remote Sens., 7 (5), 643–655.
- Topliss B. J., Almos C. L., Hill P. R., 1990, *Algorithms for remote sensing of high concentration inorganic suspended sediment*, Int. J. Remote Sens., 11 (6), 947–966.
- Wensierski W., 1983, *Light field model in the Baltic*, Stud. i Mater. Oceanol., 41, 29–62, (in Polish).
- Whitlock C. H., Poole L. R., Usry J. W., Houghton W. M., Witte W. G., Morris W. D., Gurganus E. A., 1981, *Comparison of reflectance with backscatter and absorption parameters for turbid waters*, Appl. Opt., 20 (3), 517–522.
- Woźniak B., 1977, *Influence of the sea water components on underwater light field*, Ph. D. thesis, ZO PAN, Sopot, (in Polish).

-
- Woźniak B., Dera J., Gohs L., 1977, *Attenuation and absorption of light in the Baltic water*, Stud. i Mater. Oceanol., 17, 25–51, (in Polish).
- Zalewski S. M., 1973, *An analysis of size distribution of suspended particles in sea water by electrical conductivity method*, Stud. i Mater. Oceanol., 6, 31–68, (in Polish).